Visualization of Relative Flow Patterns in Centrifugal Blood Pump

Weng Kong Chan*, S.C.M Yu, L.P. Chua and Y.W. Wong
School of Mechanical & Production Engineering, Nanyang Technological University, Republic of Singapore

This paper presents computational and flow visualization results on a centrifugal blood pump. 4 impeller designs were tested at a rotational speed of 2000 rpm using blood analog as working fluid. All impellers have seven blades but of different geometry (Impellers A3, A4, B2 and R7). Flow visualization within the impeller passages was conducted using an image de-rotation system. A pair of large scale vortices was found within the blades of impeller R7 while a single vortex was found in most of the passages of backward facing impellers (Impellers A3, A4 and B2). To establish the effects of blade geometry on blood cells, CFD was used to simulate the blade to blade flow to provide an estimate of the maximum shear stress. The results showed that though most of the stresses within the blade passages are below a threshold level of 150 N/m^2 for extensive erythrocyte damage to occur, there are some regions near to the leading edge of the pressure side where the shear stresses are above threshold level.

Key Words : Relative Flow, Centrifugal Blood Pump

1. Introduction

Recently, the use of rotary blood pumps as cardiac assist devices are gaining popularity due to improved design of the drive system. Previously, problems such as hemolysis and thrombus formation at the interface of the rotating shaft and bearings have limited the use of rotary blood pumps to less than 2 days. Innovative drive systems such as the magnetically suspended centrifugal blood pumps as proposed by Akamatsu et al. (1992) have alleviated these problems and they are seen as a viable candidate for permanent implant. The engineering complexity and high cost of pulsatile assist devices have accentuated the need for a simpler assist device such as the centrifugal blood pump. Although there are reports by Nakata et al. (1996) and Sezai et al. (1997) that continuous blood flow will have several detrimental physiological effects, Allen et al. (1997) have indicated that these effects are only temporary. Despite these controversies, it is certain that non-pulsatile flow is not a limiting factor to maintain life as reported by Yada et al. (1983) and Minami et al. (1992). Thus, centrifugal blood pumps have gained increasing acceptance due to their ease of applications, relative low cost, simplicity, small size and ability to generate high flow rates. However, the development of a cost effective, reliable and durable centrifugal blood pump as described by Akamatsu et al. (1995) is a difficult task due to the complexity of blood as working medium. Design criteria require compromises that are both demanding and conflicting. In general, a left ventricular assist device must generate a flow rate of about 5 l/min and a pressure head of about 100 mmHg while minimising hemolysis and thrombus formation. The detail mechanism of blood trauma is still not fully understood. It is felt that understanding the flow patterns within the pump can lead to improvements in the pump design. The objective of the present study is to

* Corresponding Author,
E-mail : mwkchan@ntu.edu.sg
TEL : +65-7905497; **FAX** : +65-7911859
School of Mechanical & Production Engineering, Nanyang Technological University, Republic of Singapore. (Manuscript **Received** August 2, 2001; **Revised** October 16, 2001)

couple CFD and flow visualization techniques to examine the flow characteristics between the impeller blades of a centrifugal blood pump model. Flow visualisation is an inexpensive and relatively easy method to provide the designer with a global picture of the flow pattern without resorting to expensive and time consuming detailed velocity measurements. It was observed that for the same inlet and outlet blade angles, the blade profile is critical in changing the flow pattern in the blade passages and hence the shear stresses acting on red blood cells.

2. Experimental Setup

An acrylic model of a centrifugal blood pump (1:1 scale) was tested in a closed circuit loop as shown in Fig. 1. The close-loop circuit consisted of a fluid reservoir, a throttle clamp, pressure transducers and a flow probe. Blood analog, using a mixture of glycerine and water and having a dynamic viscosity of 3.5 centipoise, was used as working fluid. The impeller, with a height of 3.5 mm, has inner and outer diameters of 13 mm and 25 mm respectively. For this study, four impellers with different blade profiles were studied for a given volute. They are shown in Fig. 2. The first three impellers are backward facing impellers (A3, A4 and B2) with same inlet and outlet blade angles of 6.74° and 30° respectively. The main difference between these impellers is the shape of the blade profile. These impellers were designed using the inverse design method which was first proposed by Borges (1990) and further refined by Li (1999). This technique uses a prescribed mean swirl $r\overline{V}_\theta$ distribution as input, i. e., radius times tangential velocity, throughout the meridional section of the pump. The last impeller (R7) is a straight radial blade impeller with inlet and exit blade angles of 90°.

Analysis of the relative flow patterns between the blades of an impeller is difficult when an observer remains stationary relative to the impeller. However, when the observer rotates with the impeller at the same speed, the relative flow field can be observed. Without having the observer to rotate with the impeller, the relative

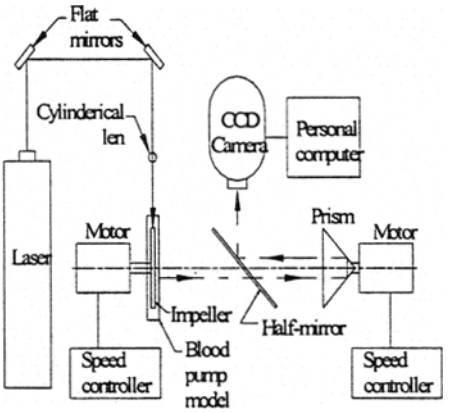

Fig. 1 Flow visualisation setup

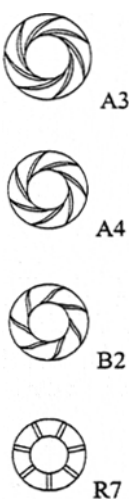

Fig. 2 Impeller Configurations

flow field in an impeller can be obtained through the use of an image de-rotator (Ohki, 1983) as illustrated in Fig. 3. It optically "freezes" the image of the rotating impeller, which is then analyzed by flow visualization to provide flow patterns within the blades. It is noted that regardless of the orientation of the object 'F', a laterally inverted image of the object 'F' is obtained. Therefore, for an object rotating at a certain angular velocity, the image of a rotating object will always be upright but inverted and stationary in real time if the image de-rotator rotates in the same direction but at half the speed of the object. This technique had been adopted by several other researchers (Fagan, 1981 and

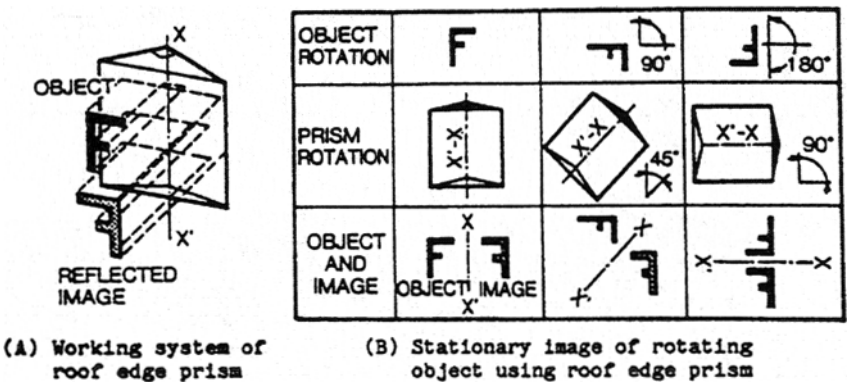

Fig. 3 Optical principle of image de-rotator [Taken from Minami et al.(1992)]

Waddell, 1976).

To render the flow pattern visible, 50 μm polystyrene spheres of were used as tracers. To illuminate the pump, a 2.5W argon-ion laser operated in continuous mode was transformed into a light sheet of 1-mm thick. The tracer particles in the plane of the light sheet were then observed and photographed. The flow patterns within the illuminated region of interest i. e. the blades of the impeller, can be viewed by a CCD video camera via a beam-splitter. This camera has a frame rate of 25 per second with monochrome high resolution of 768 by 576 pixels (JAI, CV-3000). An image acquisition board (MV-1000) was used to digitize the analog camera video output into 8 bits pixel at rates up to 40 million samples per second.

The volume flow rate was determined by an electromagnetic blood flow meter (Nihon Kohden MFV-3200). This flow probe provided accurate blood flow measurement with an accuracy of within $\pm 5\%$. The pressure developed by the pump is measured using pressure transducer (Druck DPI 260 series Digital Pressure Indicator) which has an accuracy of $\pm 0.04\%$ full scale.

3. Numerical Simulation

Experimentation is a costly and time consuming affair. Before deciding on the impellers to be tested, CFD simulation using a commercial software FLUENT (1995) was carried out to model the flow pattern in the blade passage. It is a well-known fact that in centrifugal impellers, the axial velocity component can be neglected as compared to the radial and angular components. Hence, it was reasonable to simulate the passage flow as a 2D problem. In these circumstances, the flow at the mid-span was representative of the velocity field. To maintain accuracy at the wall boundaries, boundary-fitted grids were used such that discretized boundaries coincide with mesh points used in the numerical solution. Grids were also refined near the region of extension area, blade wall and in areas where high velocity were anticipated. The total number of nodes for each blade passage was about 6283 referred to as standard grid size. There were 21 nodes in both the inlet and outlet extensions and 61 nodes on the blade surface, giving a total of 103 grid points in the radial direction as shown in Fig. 4. In the circumferential direction, there were 61 grid points. The calculation was performed on a Pentium-II 400MHz processor and it required about 10000 time-steps, which was approximately 6-7 hours of central processor unit (CPU) time. To check for mesh independency, an additional denser mesh of 12300 grids was generated and the flow field was computed at similar conditions as the standard mesh. In general, the overall flow patterns of finer grid calculation did not differ from that of the standard mesh. Thus, simulation was performed using the standard grid.

Like any flow analysis in turbo-machinery, it is convenient to solve the governing equations in a

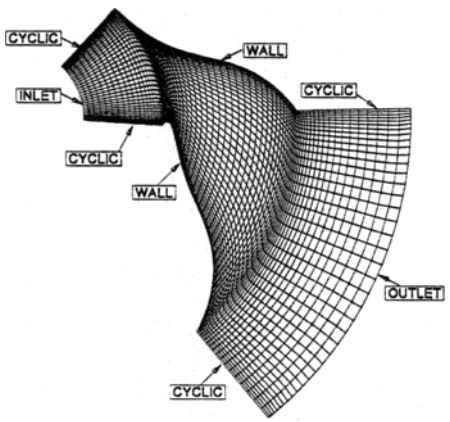

Fig. 4 Boundary conditions used for impeller passage

rotating frame of reference. This will allow a clearer understanding of the relative flow in the blade passage, which is assumed to be steady. Therefore there was a need to modify the equations of motion to accommodate the transformation to an inertial frame. The additional terms due to Coriolis forces are taken care of when a rotating frame of reference is specified. The RSM model was used instead of the standard κ-ε turbulent model (Lakshminarayana, 1996) since the Reynolds number based on the angular velocity and the outer impeller diameter was approximately 40000. The flow inside the blade passage may be turbulent due to the geometrical complexity and rotational effect. Therefore, laminar flow model was not used to simulate highly complex rotational flow in impeller. To relate the Reynolds stresses to the mean quantities, RSM was used to simulate the turbulent effect of flow within the blade passages. This model employed the transport equations governing the individual Reynolds stress components, which were then substituted into the turbulent momentum equation.

At the inlet of the computational domain, an inlet relative velocity was prescribed with the assumption of no pre-rotation. The inlet velocity encompassed of a normal velocity, which was in the radial direction and has a magnitude such that the flow rate corresponds to 5 L/min, and a tangential velocity based on design rotating speed. At the outlet, the relative pressure is set to zero. At the blade surface, the wall was defined with zero velocity. It was assumed that the fluid was circumferentially periodic and invariant with flow passages, thus CYCLIC boundary conditions were specified at the two sides of the extension areas. All velocity components, pressure, turbulence kinetic energy and dissipation rate were the same on the CYCLIC boundaries. This permitted the simulation of only one of the seven blade passages of an impeller. The values for the turbulent kinetic energy κ and its dissipation ε at the inflow boundary were set according to the following relations:

$$\kappa=\frac{3}{2}(T_u * u_{mean})^2$$

$$\varepsilon=C_u^{3/4}\frac{\kappa^{\frac{3}{2}}}{0.07L}$$

where

C_μ is an empirical constant (C_μ=0.09), Tu is the turbulence intensity, which is assumed to be 2%, L is the length scale characteristics of the turbulence, which is assumed to be the inlet radius of the extension region and U_{mean} is the mean velocity. The values of density (ρ) and dynamic viscosity (μ) of the medium were taken to be 1050 Kg/m^3 and 3.5×10^{-3} Kg/ms respectively to approximate blood properties under normal body temperature.

4. Results and Discussion

Due to the fact that the flow field is in the rotating frame of reference, both a radial velocity and a tangential velocity are prescribed at the INLET. Velocity vectors at the OUTLET seem to be tangential as the radial velocity components is of much smaller magnitude when compared to the tangential components. Mass conservation was observed and the difference between the inlet and outlet mass flow rate is less than 2%.

The relative flow patterns in the passages of the four impellers (A3, A4, B2 and R7) are shown in Fig. 5. In the figure, the blade rotates in the clockwise direction. All experiments were conducted at a rotational speed of 2000 rpm and

Fig. 5 Relative flow patterns in blade passages

a flow rate of 5 L/min. The shutter speed of the camera was set to $1/500^{th}$ of a second. It was observed that in R7, there exists a pair of large-scale vortices at the suction side while the bulk flow goes smoothly along the pressure side. In the case of radial blade impeller where the inlet blade angle is 90°, the relative velocity vector at the inlet will always differ from the blade angle, thus giving rise to flow separations at the inlet of the suction side. The vortex appearing near the leading edge of the suction side is largely due to the mismatch between the inlet flow and blade angles. The second vortex near the trailing edge of the suction side is due to adverse pressure gradient. For backward facing blade profile, it was observed that the number of vortices and the size of the vortex are very different from that of the radial blade. Unlike the impeller R7 where the vortices are formed at both the leading and trailing edges of the suction blade, there is no vortex formation at the leading edge of backward facing impellers (A3, A4 and B2) due to the smaller difference between the inlet flow and blade angles. It is evident that flow separation does not occur at the leading edge of the suction side because flow at design condition seems to be better aligned with the inlet blade angle. It is observed that the flow patterns within the blade passages are qualitatively similar to each other with the vortex being confined to the region near the trailing edge of the suction blade and the main flow is attached along the pressure side in each sector. The formation of the vortex is more likely due to the adverse pressure gradient causing the flow to separate.

The computed velocity distributions in a single passage of impellers R7, A3, A4 and B2 are presented in Fig. 6. In the case of impeller R7, a pair of strong re-circulating vortices indicated by the letters 'A' and 'B' is observed within the blades. The flow is restricted to the pressure side of the blade passage. The formation of vortex A is mainly due to the difference in the relative flow angle and blade angle, while vortex B is due to the adverse pressure gradient on the suction side. Flow pattern obtained experimentally is similar to the computed flow field. A large vortex B and a smaller vortex A near the impeller outlet are observed for impellers A3, A4 and B2. The main flow is also restricted to the pressure side. In general, the flow pattern is qualitatively similar to the predicted flow field for all the impellers revealing the dominance of the vortex B. The small vortex A predicted by CFD is not obvious in experimental flow visualization. The agreement between the numerical simulation and experimental flow visualization results are reasonably good. Through observations of flow patterns, blood trauma can be anticipated by identifying the region of re-circulation. However this does not quantitatively indicate the level of damage imposed onto the blood cells. Based on the velocity profiles, the shear stresses in the blade passages were computed and presented in Fig. 7. It was noted that for majority of the regions within the blade passages, the shear stresses were found to be less than 40 N/m^2 which is below the threshold level of about 150 N/m^2 (Leverett et al, 1972). The maximum shear stress which is defined as the sum of the laminar and turbulent shear stresses was also determined. The numerical simulations showed that the maximum shear stress within the blade passages for impellers R7, A3, A4 and B2 are all below 240 N/m^2. There are few regions within the blades that are associated with high shear stress. One particular high shear stress region is at the wall of the pressure side nearer to the blade inlet radius. It is the stagnation point where fluid particles first come into contact with the rotating blades. The fluid is reduced to rest at the blade inlet radius. Another region that induces high shear stress is at the pressure side. The fluid near the wall of the pressure side produces a very high velocity gradient due to the viscous effects. This results in a high shear region near the whole blade length in the pressure side. The interface between the high velocity main flow and the re-circulating vortices

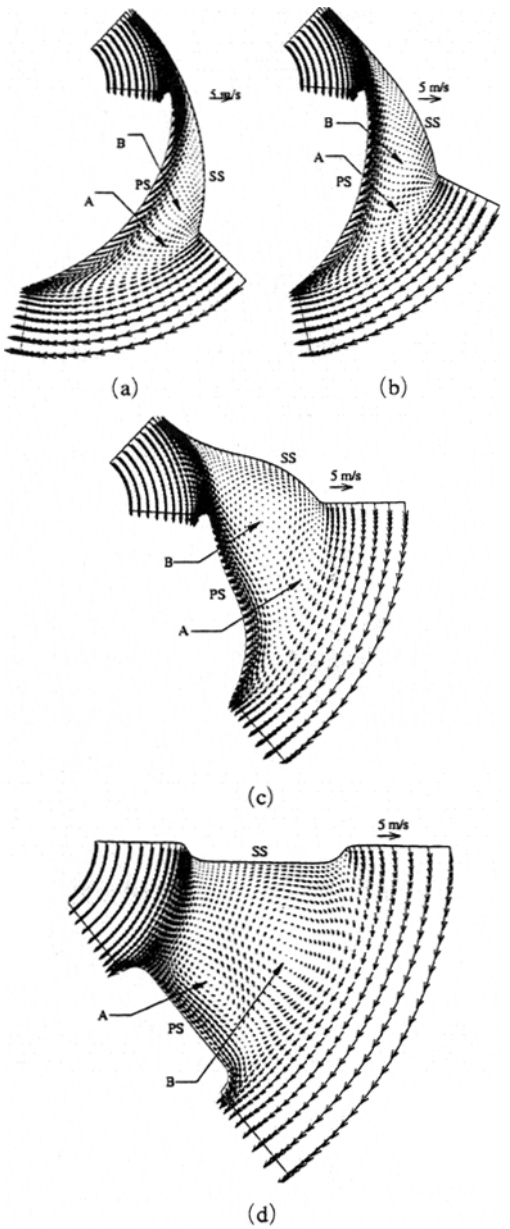

Fig. 6 Velocity distribution

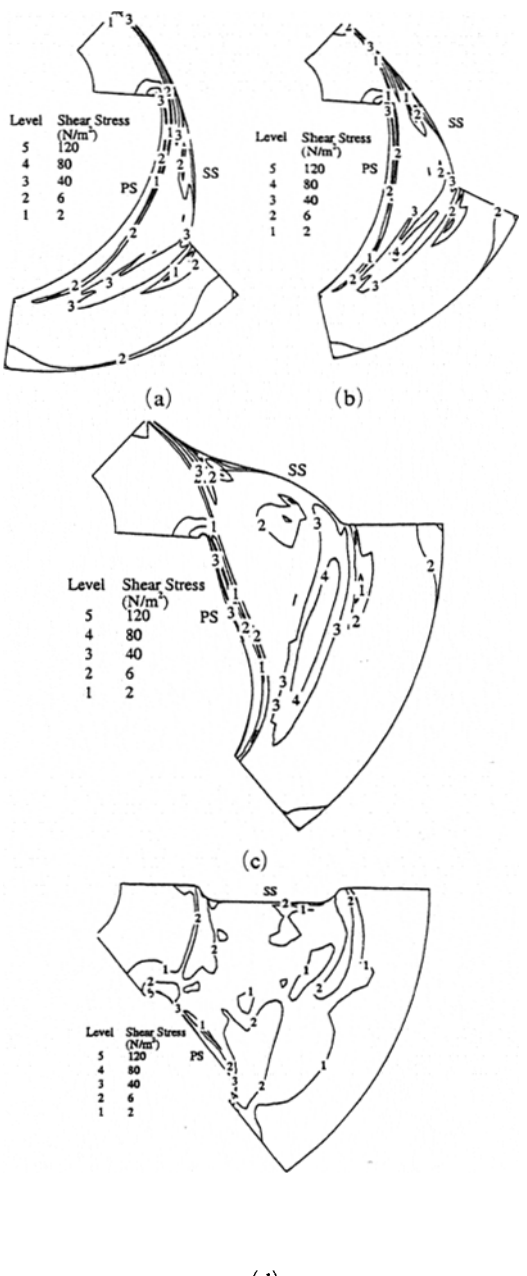

Fig. 7 Shear stress distribution

is another area where higher shear stress can be anticipated. At the interface between the pair of re-circulating vortices is another potential site of high shear stress. Though these results are above the threshold level of 150 N/m^2, these high shear stresses may not cause irreversible damage to blood cells, as these happened only for a short period of time.

5. Conclusions

In this present investigation, the influence of impeller blade curvature on the flow pattern was investigated both computationally and experimentally. It was noted that for the four impellers

investigated, flow was restricted to the pressure side of the blade while flow separation occurred on the suction side. The location of the vortex center is an ideal site for thrombus formation due to the low velocity fluid at the core. Comparison of flow patterns between experimental flow visualization and numerical simulation were made and were qualitatively in good agreement. An important factor to be considered in blood pump design is the amount of damage sustained by blood cells in the pump. Though the quantification of blood trauma has yet been realized, numerical simulation provided an improved insight into the velocity and shear stress distributions within the blades.

References

Akamatsu T., Nakazeki T. and Itoh H., 1992, "Centrifugal Blood Pump with a Magnetically Suspended Impeller." *Artificial Organs*, Vol. 16, No. 3, pp. 305~308.

Akamatsu T., Tsukiya T., Nishimura K., Park C. H. and Nakazeki T., 1995, "Recent Studies of the Centrifugal Blood Pump with a Magnetically Suspended Impeller," *Artificial Organs*, Vol. 19, No. 7, pp. 631~638.

Allen G. S., Murray K. D. and Olsen D. B., 1997, "The Importance of Pulsatile and Nonpulsatile Flow in the Design of Blood Pumps," *Artificial Organs*, Vol 21, No. 8, pp. 922~928.

Borges J. E., 1990, "A Three-Dimensional Inverse Method for Turbomachinery: Part I-Theory," *Journal of Turbomachinery*, Vol 112, pp. 346~354.

Fagan W. F., Beeck M. A. and Kreitlow H., 1981, "The Holographic Vibration Analysis of Rotating Objects Using a Reflective Image De-rotator," *Optics and Lasers Engineering*, Vol 2, pp. 21~32.

FLUENT Version 4. 3 User's Guide, 1995, *Fluent Inc.*

Lakshminarayana B., 1996, *Fluid Dynamics and Heat Transfer of Turbomachinery*. Wiley & Sons New York.

Leverett L. B., Hellums J. D., Alfrey C. P. and Lynch E. C., 1972, "Red Blood Cell Damage by Shear Stress," *Biophyscial Journal*, Vol 12, pp. 257~272.

Li H. D., 1997-99, "Inverse Design and Optimization of Blood Pump Impeller using Computational Fluid Dynamics," *Final Research Report*, Nanyang Technological University.

Minami K., El-Banayosy A., Posival H., Seggewi(H., Murray E., Korner M. and Korfer R., 1992, "Improvement of Survival Rate in Patients with Cardiogenic Shock by using Nonpulsatile and Pulsatile Ventricular Assist Device," *Int. Journal of Artificial Organs*, Vol 15, No. 12, pp. 715~721.

Nakata K., Shiono M., Orime Y., Hata M., Sezai A., Saitoh T. and Sezai Y., 1996, "Effect of Pulsatile and Nonpulsatile Assist on Heart and Kidney Microcirculation with Cardiogenic Shock," *Artificial Organs*, Vol 20, No 6, pp. 681~684.

Ohki H., Yoshinaga Y. and Tsutsumi Y., 1983, "Visualization of Relative Flow Patterns in Centrifugal Impellers," *Proceedings of the 3rd International Symposium on Flow Visualization*, pp. 723~727.

Sezai A., Shiono M., Orime Y., Nakata K., Hata M., Yamada H., Ida M., Kashiwazaki S., Kinishita J., Nemoto M., Koujima T., Sezai Y. and Saitoh T., 1997, "Renal Circulation and Cellular Metabolism During Left Ventricular Assisted Circulation: Comparison Study of Pulsatile and Nonpulsatile Assists," *Artificial Organs*, Vol 21, No. 7, pp. 830~835.

Waddell P., 1976, "Epicyclic Motion: A System for Real Time Examination," *Engineering Materials and Design*, Vol. 20, pp. 2~4.

Yada I., Golding L., Harasaki H., Jacobs G., Koike S., Yozu R., Sato N., Fujimoto L., Snow J., Olsen D., Murabayashi S., Venkatesen V., Kiraly R. and Nose Y., 1983, "Physiopathological Studies of Non-pulsatile Blood Flow in Chronic Models," *ASAIO*, Vol. 29, pp. 520~525.